Composites Part B 282 (2024) 111535

Contents lists available at ScienceDirect

Composites Part B

journal homepage: www.elsevier.com/locate/compositesb

Pressure resistance characterisation of vascular networks embedded in carbon composites for high energy physics applications

M. Dias [a,c], D. Alvarez [a], F. Boyer [a], H. Lu [b], P. Olivier [c,**], L.R. Pickard [b,*], B. Teissandier [a]

[a] European Organization for Nuclear Research (CERN), Switzerland
[b] Bristol Composites Institute, Aerospace Engineering Department, University of Bristol, England, UK
[c] Institut Clément Ader (ICA), Université de Toulouse, CNRS, France

ARTICLE INFO

Keywords:
Mechanical testing
Fracture
Braiding)

ABSTRACT

In state-of-the-art tracking detectors, lightweight carbon composite structures support the pixel or micro-strip sensors and provide the main thermal path between the silicon and a network of metallic or plastic pipes containing a cooling fluid. Despite the good results obtained with this design approach, the challenges associated with future high energy physics (HEP) experiments demand even lighter and more efficient technologies. In this regard, replacing the existing piping with a network of channels directly embedded in the composite laminates represents a promising solution to improve the thermal coupling, which also offers additional gains in terms of mass and thermo-elastic stability.While some research has been devoted to assessing the mechanical and thermal performance of such laminates, limited information about their resistance to internal pressure is currently available in the literature. This lack of data constitutes an important obstacle for the use of vascular networks in future HEP applications, which the present paper aims to address.Experimental methods were used to investigate the pressure resistance of channels embedded in carbon composite laminates. Modified poly (lactic) acid (PLA) preforms were embedded in carbon-fibre epoxy laminates. A post-cure vaporization technique removed the PLA, thus producing plates with longitudinal channels. Destructive tests were conducted to determine the burst pressure of the plates depending on the lay-up and the cross-section geometry of the channels. Both circular and oblong channels were evaluated, and various reinforcement techniques were explored to enhance the pressure resistance of the laminates. Micro-graphic examinations and X-ray micro-computed tomography were employed to gain a better understanding of the microstructure and the failure mechanisms of the plates.Plates with circular channels measuring 1.75 mm in diameter, embedded in $[0/90/0]_S$ laminates and reinforced with 2 mm lay length fuzzy carbon fibre over-braids, achieved burst pressures exceeding 45 MPa. This result, which is approximately an order of magnitude greater than that obtained for the equivalent non-reinforced laminates, demonstrates the enormous potential of this technology for future particle detectors.

1. Introduction

At the core of high energy physics (HEP) experiments such as those installed at CERN's Large Hadron Collider (LHC), particle detectors probe the byproducts of the collisions between two particle beams which travel in opposite directions at close to the speed of light. Alternatively, the high-energy beam is directed to a fixed target to produce secondary particles for specific studies. In both cases, the detectors measure key characteristics of the particles created in the collisions (momentum, energy, mass) to identify their type [1].

Modern HEP experiments consist of multiple layers of sub-detectors, each conceived to look for specific properties or particular types of particles. Specifically, advanced silicon trackers rely on thousands of micro-strip and/or pixel sensors disposed in several layers to reconstruct the trajectory of electrically charged particles as they travel inside a strong magnetic field [2–4]. The arrangement of the sensors in the detector volume is conceived to optimise the tracking efficiency, spatial resolution and coverage of particle tracks. Overlaps between adjacent sensors and layers ensure the hermeticity of the layout, guaranteeing a minimum number of hits for optimal track reconstruction.

* Corresponding author. Bristol Composites Institute, Aerospace Engineering Department, University of Bristol, Queen's Building, University Walk, BS8 1TR, Bristol, England, UK.
** Corresponding author. Institut Clement ADER UMR CNRS 5312, UT3, Universite de Toulouse, France.
E-mail addresses: philippe.olivier@iut-tlse3.fr (P. Olivier), laura.pickard@bristol.ac.uk (L.R. Pickard).

https://doi.org/10.1016/j.compositesb.2024.111535
Received 30 August 2023; Received in revised form 15 April 2024; Accepted 2 May 2024
Available online 27 May 2024

Due to the high radiation levels in the vicinity of the interaction point where particles collide, the accumulated damage in the silicon sensors leads to higher leakage currents, which increase with the sustained fluence [5]. Active cooling is required to remove the heat generated in the sensors and readout electronics, mitigating these effects and preventing undesirable consequences such as thermal runaway and annealing, thereby ensuring a good performance throughout the lifetime of the detector.

Lightweight structures, often referred to as "local supports", maintain the sensors in the correct positions within the detector volume. They are conceived to maximise the mechanical stability, but also play a crucial role in the thermal management of the pixel modules. To that end, their design incorporates plastic or metallic pipes to circulate a monophase or two-phase coolant [6,7] to extract the heat generated in the sensors and readout electronics. Examples of the local supports used in the ALICE ITS [4] and ATLAS Insertable B-layer [3] are shown in Fig. 1a–c and Fig. 1b–d respectively.

The properties of carbon composite materials make them particularly well-suited for tracking applications. Their low density, high radiation length, high stiffness-to-weight ratio and excellent thermal properties are ideal for the construction of local supports, where material budget, mechanical stability and heat management are top design priorities [8]. They possess low coefficients of thermal expansion (CTE), which help minimising (i) the overall thermo-elastic deformations due to temperature excursions in the detector and (ii) the stresses transferred to the silicon sensors [9]. Whilst the through-thickness conductivity of carbon composites is naturally low, very thin laminates can provide an effective heat path between the silicon modules and the coolant inside the pipe network due to their excellent in-plane thermal properties, especially if pitch fibres such as K13D are used [10]. (It should be noted that most effective solutions to increase the through-thickness conductivity in composite laminates involve the addition metal fillers that are often incompatible with the activation constraints of HEP experiments [11].) Finally, carbon composites also exhibit satisfactory radiation hardness, enabling them to function effectively in the demanding environment of a tracker detector without experiencing substantial degradation in their mechanical or thermal properties [5,12,13]. It is worth noting that the degradation observed at higher radiation doses is predominantly influenced by the performance of the resin system [5], which can be tailored accordingly [13].

However, lighter and more efficient technologies are currently investigated [14] to meet the performance targets of future HEP experiments. As the energies in colliders continue to rise, future tracker detectors will face the formidable task of handling increasingly higher particle fluxes and radiation doses [15]. Ongoing research is exploring the use of lower temperature coolants beyond two-phase CO_2 [16], but establishing a more direct thermal path between the fluid and the silicon sensors will be crucial in mitigating radiation damage and ensuring the good performance of the detectors. In this regard, replacing the plastic and metallic pipes currently used in the local supports with a network of channels directly embedded in the composite laminates represents a promising solution to improve the thermal coupling [17] (see Fig. 2). Removing the pipes and the thermal glue layer which connects them to the rest of the local supports would result in a substantial decrease in the number of radiation lengths (X/X_0), thereby enhancing the overall tracking performance [18]. Additionally, this solution would eliminate the CTE mismatch between the composite structure and the tubes, further improving the overall thermo-elastic stability of the detector.

Among the different processes described in the literature to embed channels directly in carbon/epoxy laminated parts [17,19,20], the Vaporization of Sacrificial Component (VaSC) method [21,22] offers significant flexibility for network design. This technique utilises poly (lactic) acid (PLA) preforms as sacrificial material during the lamination process, which are subsequently removed in a post-cure treatment at 200 °C to create the channels. Unlike standard PLA, the VaSC preforms undergo a pre-treatment involving the application of a metallic catalyst to enhance their thermal degradation [23–25]. Several processes for introducing the catalyst have been documented in the literature. A. P. Esser-Khan et al. [21] and H. Dong et al. [22] employed solvent swelling techniques, where the catalyst was dispersed in a trifluoroethanol (TFE)/water solution to impregnate the PLA fibres. In an improvement upon the previous method, J. F. Patrick et al. [26] utilized a solvent blending approach by sealing PLA pellets with dichloromethane. They also proposed a melt compounding method in which PLA pellets were heated and mixed before dispersing the catalyst. Recently, the

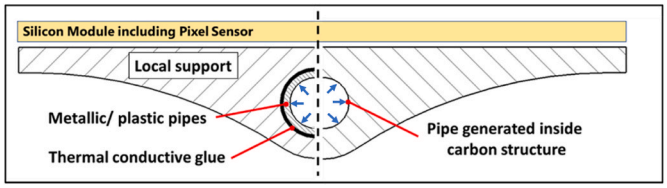

Fig. 2. Representation of local support with metallic/plastic pipes and with channel directly generated inside the structure under an internal pressure (blue arrows).

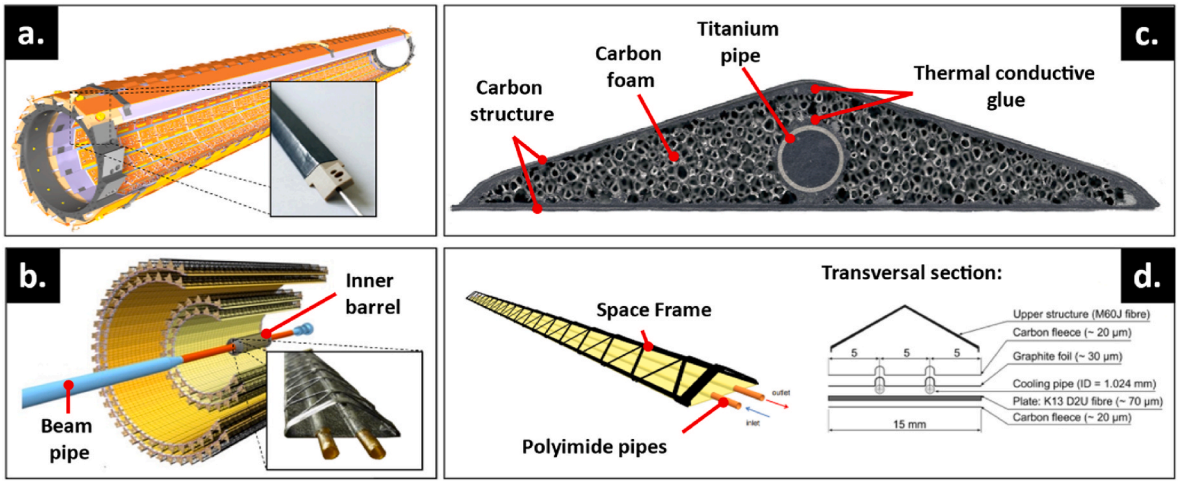

Fig. 1. (a) Representation of the Insertable B-Layer of the ATLAS experiment with the local supports (staves) layout [3]. (b) Representation of the ALICE experiment Inner Tracking System (ITS) with the local supports layout [4]. (c) Cross-section of a stave from the Insertable B-Layer of the ATLAS detector [8]. (d) Stave representation with its corresponding cross-section from the Inner Barrel of ALICE experiment [4].

vaporization of sacrificial fibers has been integrated with frontal polymerization technology to produce vascularized composites in a single step [27–29]. In the FP-VaSC process, the heat released during the curing of the host matrix system is utilized to depolymerize the embedded sacrificial preforms. These preforms are composed of poly (propylene carbonate) (PPC) modified with a photoacid generator. While the current technology readiness level of this approach is relatively low, its potential for significant energy and time savings makes it a promising alternative to the traditional two-step VaSC for future applications.

The thermo-mechanical response of carbon composite panels with vascular networks has been investigated by different research teams, primarily to experimentally assess their mechanical and thermal performance under external loads. M. W. McElroy et al. [19] and S. C. Olugebefola et al. [30] focused on the thermal behaviour of this type of panels, showing their effective heat dissipation capabilities. A. M. Coppola [31] demonstrated that panels with embedded channels for circulating coolant can maintain their stiffness integrity even when subjected to high heat loads. A. Kousourakis and co-workers [32,33] investigated the influence of channel size and orientation on in-plane tensile and compressive properties, as well as interlaminar properties. They emphasized the existence of a critical channel size from which a decline in elastic properties and interlaminar shear strength decrease significantly. Furthermore, this effect is magnified when channels are oriented transversely to the load direction. M.-U. Saeed et al. [34] summarized the effects of transversal and longitudinal channels on various mechanical properties, including interlaminar shear strength, tensile and compressive moduli and strengths, impact damage and fatigue resistance. Additionally, numerical models have been developed to simulate the response of composite laminates with embedded channels, as shown by Pety et al. [17].

This research, conducted within the framework of the CERN Strategic Programme on Technologies for Future Experiments, aimed to enhance our understanding of the mechanical performance of composite structures with embedded vascular networks. As the next generation of HEP experiments is likely to depend on high-pressure fluids for cooling, assessing the resistance of laminates to internal pressures becomes crucial. This work represents a new effort in systematically studying such unconventional load case.

PLA preforms, modified with a chemical treatment to enhance their degradation characteristics, were employed in combination with a post-cure vaporization technique to manufacture plates featuring longitudinal channels. A manufacturing method employing dedicated tooling was established to produce test specimens using different carbon materials, layups, channel cross section geometries and sizes. The samples were then tested experimentally to determine their burst pressure. The microstructure and the failure mechanisms were investigated using micro-graphs and X-ray micro-computed tomography.

The effect of different reinforcement types, including carbon and aramid overbraids, on the burst pressure of the embedded channels was also investigated. Overbraiding and overwinding are used to suppress the formation of kink bands in pultruded rod based composites to improve performance under compression [35] and compression after impact [36]. The development of 'fuzzy carbon' overbraids, utilising a combination of short lay length and the natural brittle nature of carbon fibre, results in broken fibres extending into the matrix, increasing the fibre-matrix contact region and providing shear support to the braid [37]. It is expected that the aforementioned fuzzy feature will lead to increased pressure resistance.

2. Materials

2.1. Fibre-reinforced materials

Test specimens were fabricated using both unidirectional (T800/ER450, fibre areal weight 124 g/m^2, resin content 36 %) and plain weave (T300/ER450, fibre areal weight 98 g/m^2, resin content 42 %) carbon-epoxy prepreg from Composite Materials Italy (CIT). The different layups used in the laminates are summarized in Table 1.

Two reinforcement methods were investigated to enhance the pressure resistance of the laminates with embedded channels.

- Method 1: In this approach, a ply of plain weave prepreg (T300/ER450) or a layer of dry carbon fleece (Optivel® 20301A Carbon Veil 8 g/m^2, Suter Kunststoffe AG, Switzerland) is wrapped around the sacrificial PLA preform before integrating it into the laminate. The carbon fleece was combined with an additional layer of epoxy resin (ER450, 75 g/m^2).
- Method 2: The second technique involves constructing fibre overbraids around the PLA preform prior to the lamination process [35]. Three types of over-braids were developed at the University of Bristol using carbon fibre (1k T300, Toray) with lay-lengths of 2 mm and 8 mm, as well as aramid fibre (405dtex Teijin high elongation Twaron®) with a 2 mm lay-length.

2.2. Sacrificial polylactic acid (PLA) preforms

Sacrificial PLA preforms were incorporated into the laminates and subsequently vaporised to create the channels. Before their integration, the commercial PLA fibres (4043D translucent PLA fibres with a 1.75 mm diameter supplied by NatureWorks) underwent a chemical treatment to facilitate the vaporization process. This treatment was developed at CERN and involved a solution of water and trifluoroethanol (TFE), using zinc acetate as a catalyst. A saturated solution of zinc acetate in water (430 $g.L^{-1}$) was prepared, and the necessary amount of TFE was added to achieve the desired ratio. The PLA fibres were immersed in this solution for 5 h and then dried at room temperature for 24 h.

A test campaign was conducted to evaluate the PLA solvent absorption depending on the treatment parameters. As illustrated in Fig. 3a., PLA rapidly absorbs water and TFE solution during the initial hours of soaking, with the rate of mass change gradually diminishing over time. It is also clear that a 30 % TFE solution results in a faster and greater mass uptake. Based on practical considerations, a 5-h immersion time in a 30 % TFE and water solution was chosen as the in-house reference treatment, with the mass of the PLA increasing approximately 40 % in this process. The results of the thermogravimetry analysis presented in Fig. 3b demonstrate the effectiveness of the treatment, which lowers the onset temperature of PLA degradation by 80 °C when compared to the as-received fibres (i.e. from 280 °C to 200 °C). Based on these findings, the carbon-epoxy laminates underwent a vacuum process at 200 °C to eliminate the preforms, leaving behind the desired empty channels.

As depicted in Fig. 4, three types of PLA preform were employed to obtain different channel geometries: (a) Circular channels with a diameter of 1.75 mm (hydraulic diameter: $D_H = 1.75$ mm), (b) oblong channels with a width of 3.5 mm (hydraulic diameter: $D_H \approx 5.5$ mm), and (c) oblong channels with a width of 5.25 mm (hydraulic diameter: $D_H \approx 7.5$ mm). For the oblong channels, two or three circular PLA fibres with a 1.75 mm diameter were combined to create the preforms. Specific moulds were developed to pre-shape these preforms in the oven (175 °C,

Table 1
Lay-ups and materials used in the laminates. In all cases, the PLA preform is positioned in the symmetry plane.

Layup	Material
$[0/90/0]_s$	T800/ER450 UD
$[90/0/90]_s$	T800/ER450 UD
$[0/90/90/0]_s$	T800/ER450 UD
$[90/0/0/90]_s$	T800/ER450 UD
$[\pm45/\pm45/\pm45]_s$	T300/ER450 plain weave

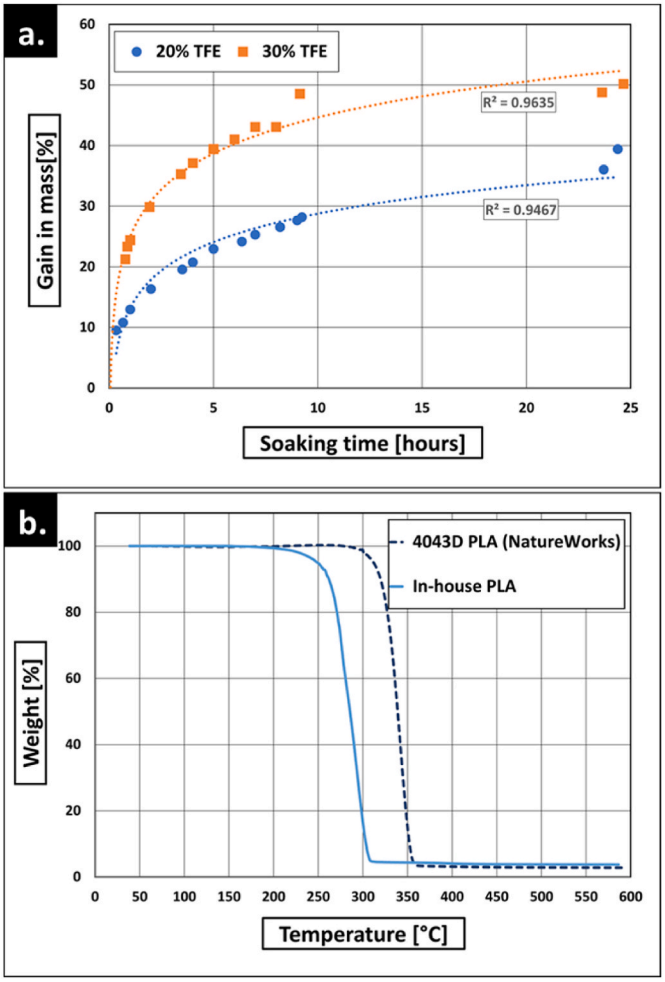

Fig. 3. a) Change in mass of 1.75 mm diameter PLA fibres as a function of the soaking time in a TFE:water solution for two different TFE concentrations. (b) Thermogravimetry results comparing two types of PLA fibre: untreated (4043D PLA NatureWorks) and treated at CERN (in-house PLA).

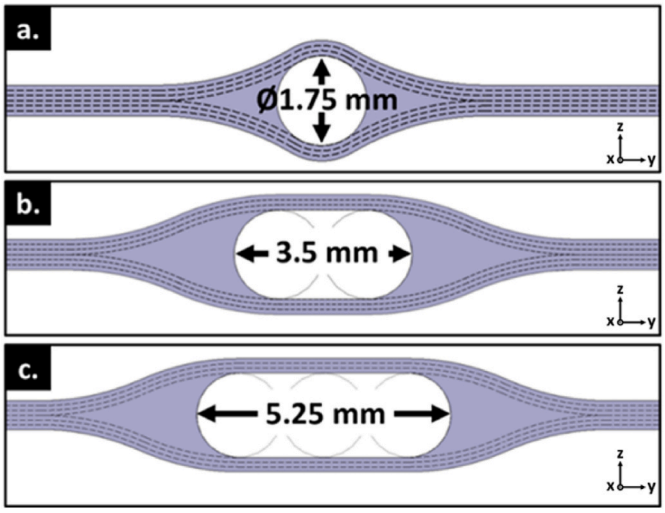

Fig. 4. Cross-section representation of three different channel shapes (i.e., PLA preforms) embedded within carbon/epoxy laminates: (a) Circular channel with a diameter of 1.75 mm, (b) oblong channels with 3.5 mm and 5.25 mm widths and 1.75 mm height.

60 min) with the help of a vacuum bag. Narrower, circular channels are expected to result in higher burst pressures, while oblong cross sections offer potential advantages in terms of hydraulic diameter, thereby reducing pressure drops in the cooling circuit without affecting the total thickness of the composite plates. The dimensions of the channels chosen for this study align with those found in state-of-the-art silicon detectors, which typically utilize metallic and plastic pipes with hydraulic diameters ranging from 0.5 mm to 2.5 mm [3,4,7,38,39].

3. Manufacturing laminates with embedded channels

In this section, the various steps of the manufacturing process to obtain the final laminates with embedded channels are outlined.

3.1. Ply collation, moulds, and curing

Cross-ply and angle ply laminates were manufactured using T800/ER450 unidirectional and T300/ER450 plain weave prepreg plies according to the stacking sequences specified in Table 1. Aluminium moulds with machined grooves were used to facilitate the integration of PLA fibres on the laminates, which were placed on the mid-plane in all cases (see Fig. 5a–c.). It is important to underline that the longitudinal axis of the PLA preform corresponds to the fibre reference direction (i.e. 0°). As such, in $[0/90/0]_s$ and $[0/90/90/0]_s$ laminates the fibres in the first ply at either side of the mid-plane are parallel to the PLA preform, whilst in $[90/0/90]_s$ and $[90/0/0/90]_s$ laminates they are perpendicular. Fig. 6 clearly shows the consequences of these arrangements on the composite microstructure. All laminates were autoclave-cured according to the cycle depicted in Fig. 7, which follows the recommendations of the prepreg manufacturer (2 h at 135 °C) [40].

Differential Scanning Calorimetry (DSC) measurements were conducted on samples extracted from the laminates, which yielded a glass transition temperature (T_g) of 172 ± 8.25 °C and a degree of cure (α) of 97 ± 0.25 %. Microscope imaging analysis was employed to determine the fibre volume fractions (V_f) away from the PLA preform, resulting in $V_f = 61$ % for the 8-ply laminates and $V_f = 59$ % for the 6-ply laminates.

3.2. Manufacturing of plates with manually reinforced channels

To meet the pressure requirements of future HEP experiments, various local reinforcement techniques were developed to strengthen the final channels and enhance the pressure resistance of the laminates. As discussed in section 2, three types of reinforcements were studied, namely: carbon fleece, T300/ER450 carbon plain weave prepreg ply, and carbon or aramid over-braids. During the manufacturing process, a T300 carbon woven ply was wrapped around the PLA preform once (see Fig. 8a and Fig. 8b.). The carbon fleece was wrapped around the PLA twice, introducing an additional layer of ER450 resin film (see Fig. 8c.). In all cases, the reinforced PLA preforms were positioned on the laminate mid-plane before the curing.

3.3. Manufacturing of overbraided reinforcements

The carbon and aramid over-braids were produced directly over the PLA at the Bristol Composite Institute, UK (Fig. 8d and e.). Overbraiding was carried out using a Herzog 1/16/80 circular maypole microbraider run at half capacity, using 8 tows evenly spaced in the braider rather than the full 16. This allows the material to braid around the 1.75 mm diameter PLA while minimising bunching at short lay length. A diamond interlacement pattern was produced, following the method of O'Keeffe et al. [41], with the PLA fed through the centre of the braider from below. Two lay lengths were used.

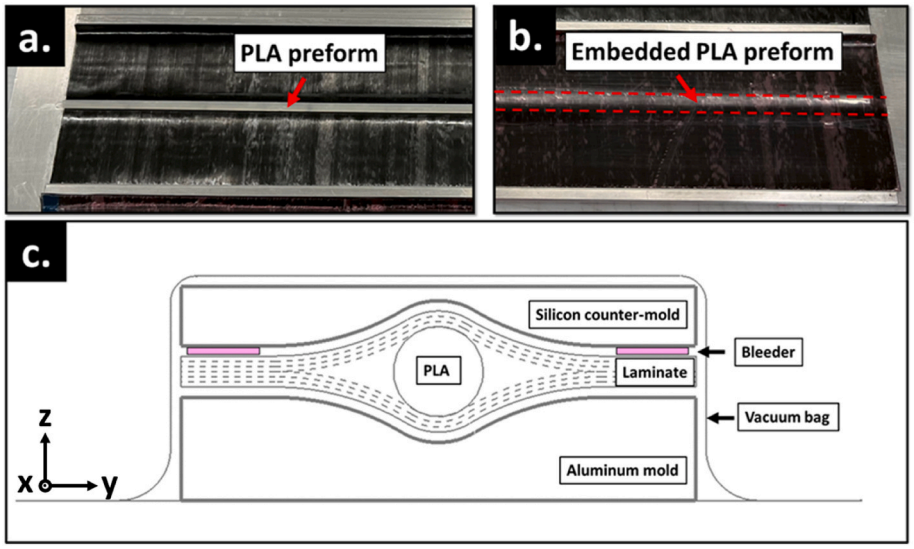

Fig. 5. (a) Placement of the PLA preform during the lamination process. (b) PLA preform embedded in the carbon laminate before curing. (c) Schematic cross-section of the 6-ply carbon/epoxy laminates (shown in grey, with dashed lines representing the plies) with embedded channels obtained through the vaporization of the corresponding sacrificial PLA preforms.

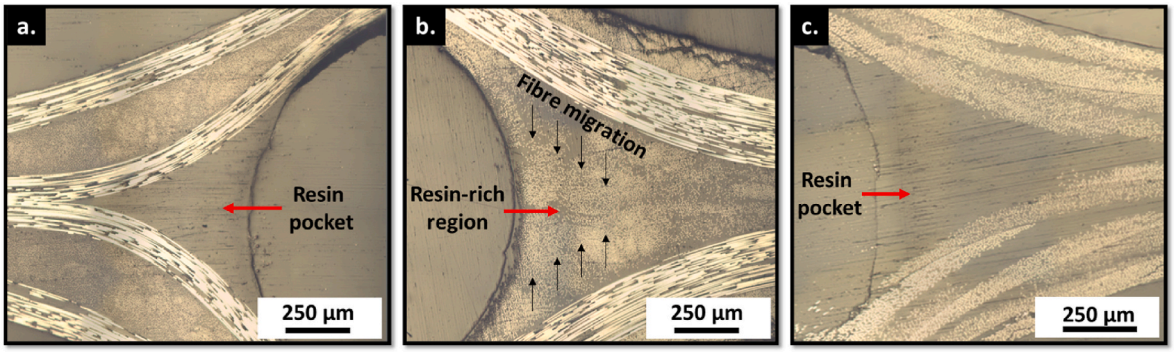

Fig. 6. (a) Microstructure of laminates with a 90°/90° interface, revealing the presence of resin pockets around the channel. (b) Microstructure of laminates with a 0°/0° interface, exhibiting fibre migration towards the mid-plane. (c) Microstructure of T300 laminates with resin pockets in the vicinity of the channel.

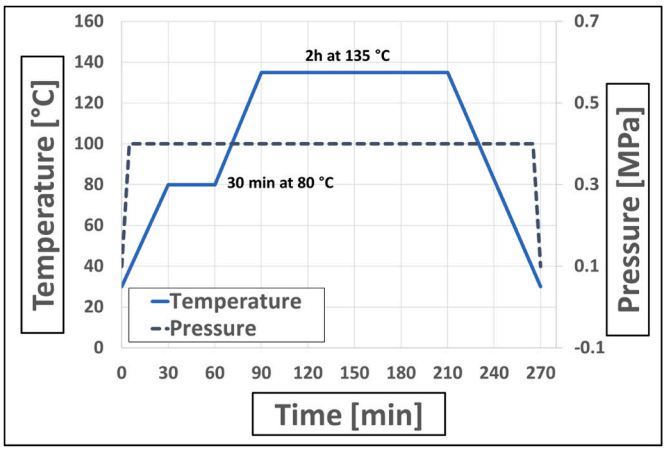

Fig. 7. Autoclave curing cycle used for the test specimens.

a) 2 mm lay length, which can be used to produce the 'fuzzy' effect with T300 carbon. This was also used with High Elongation Twaron (aramid yarn).
b) 8 mm lay length, with T300 carbon only, for comparison to the 2 mm lay length.

For the oblong PLA samples, the 8 mm lay length T300 carbon fibre did not provide full coverage of the PLA therefore there are expected to be gaps in the reinforcement.

The overbraided PLA was integrated into the test panels as detailed above (i.e., in the laminate mid-plane), with a length of braid protruding to minimise the risk of fraying during the manufacturing process (see Fig. 9).

3.4. Creation of the channels: post-cure PLA vaporization step

Once cured, all the plates were transferred to a vacuum oven, where they were exposed to a temperature of 200 °C for a period of 15 h to facilitate the complete degradation and removal of the PLA preforms. After the vaporization step, compressed air was flushed into the generated channels to remove any potential PLA residue.

3.5. Quality control of the laminates with embedded channels

To validate the manufacturing process and assess the quality of the channels, the final plates were examined using X-ray micro-computed tomography. Fig. 10 illustrates the results obtained for plates containing unreinforced circular and oblong channels. This analysis enabled the observation of well-preserved and uniform channels in plates up to 600 mm in length, with minimal porosity. However, the microstructure

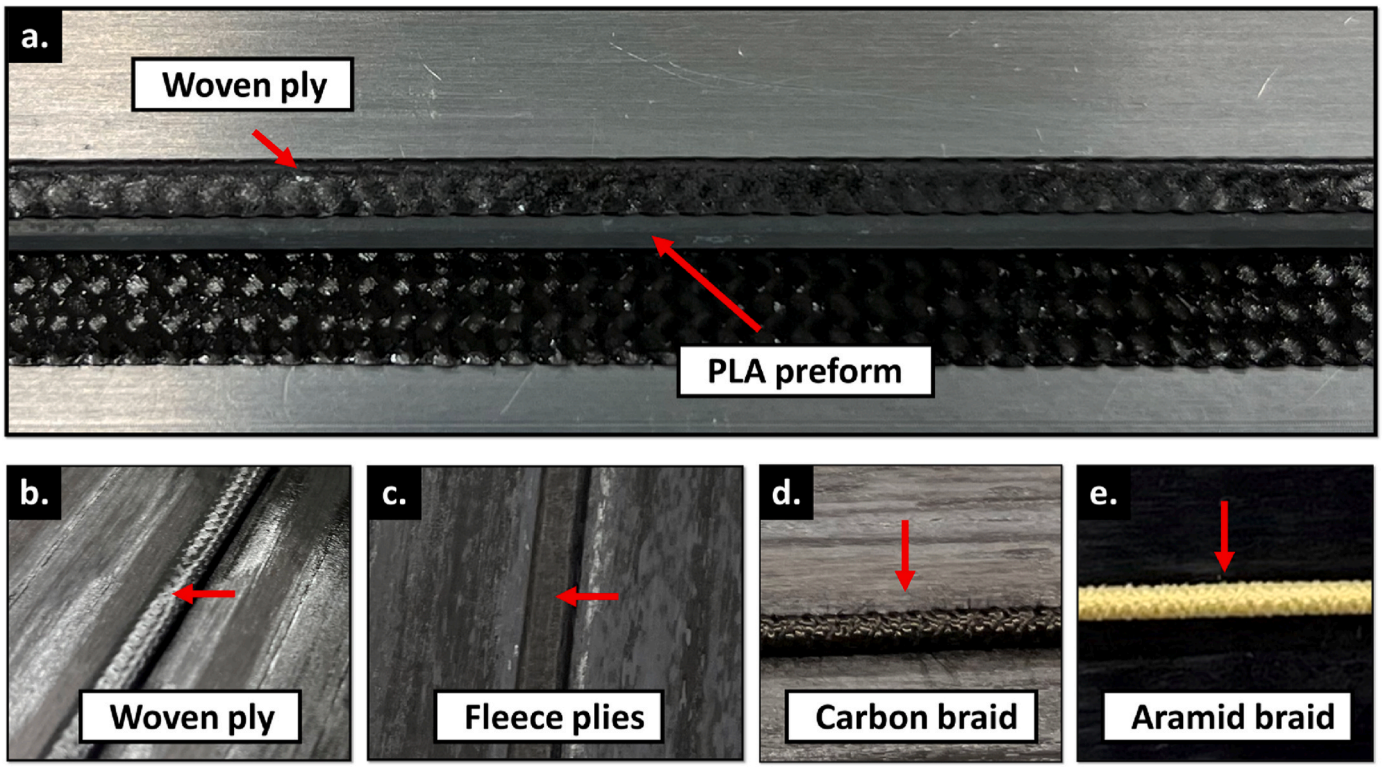

Fig. 8. (a) Woven ply wrapped around an oblong PLA preform. (b) PLA preform with a carbon woven reinforcement installed in the laminate. (c) PLA preform with carbon fleece reinforcement. (d) T300 carbon over-braid with 2 mm lay length. (e) Aramid braid.

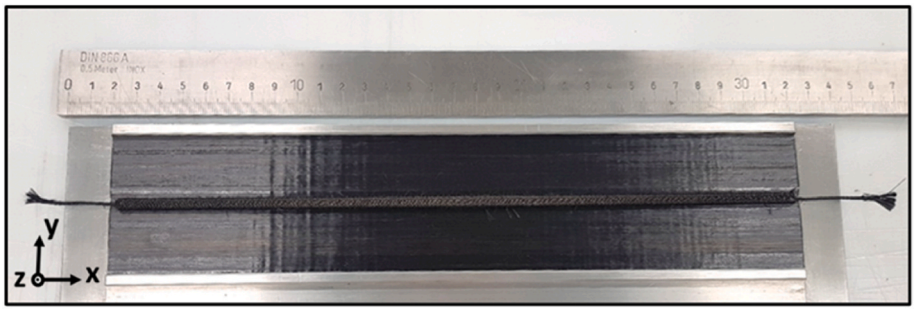

Fig. 9. Overbraided PLA with 2 mm lay length carbon fibres placed in the middle of the plate during lamination.

surrounding the channels was not clearly discernible due to limitations in the tomography technique. To overcome this limitation, additional micrographic examinations were conducted to gain further insights into the composite microstructure, particularly in the vicinity of the channels (see Fig. 6).

3.6. Preparation of the test samples for pressure tests

After the vaporization step, the composite plates were cut using a dry saw to obtain 140 mm long and 45 mm wide test samples. Stainless steel needles were inserted at the extremities of the embedded channels and bonded to the plates with a two-part epoxy adhesive (Araldite 2011). Aluminium or PEEK tubes were bonded to the needles to interface with single-ferrule fittings.

Finally, one side of the samples was coated with a thin layer of white paint. Black speckles were deposited on the white background with a spray gun to create a high-contrast, random pattern.

4. Experimental methods

The samples were mounted on a dedicated test bench and clamped at both extremities. One side of the channel was connected to a manually operated, hydraulic pump (Fluke 700HTPK-2) with a water reservoir, while the opposite end was blocked with a closed valve. A sensor installed at the inlet (Fluke 700G) was used to measure the pressure in the circuit (see Fig. 11). The water pressure was gradually increased, ensuring quasi-static loading conditions. The burst pressure was determined by observing a sudden drop in the pressure sensor reading or upon visual detection of a leak.

A Digital Image Correlation (DIC) system (Dantec Dynamics Q400) was used to monitor the strain field in the composite samples during the pressure tests.

X-ray micro-computed tomography was performed using a Zeiss METROTOM 1500 CT scanner with a voxel size comprised between 7 μm and 45 μm, depending on shape control or crack path purposes.

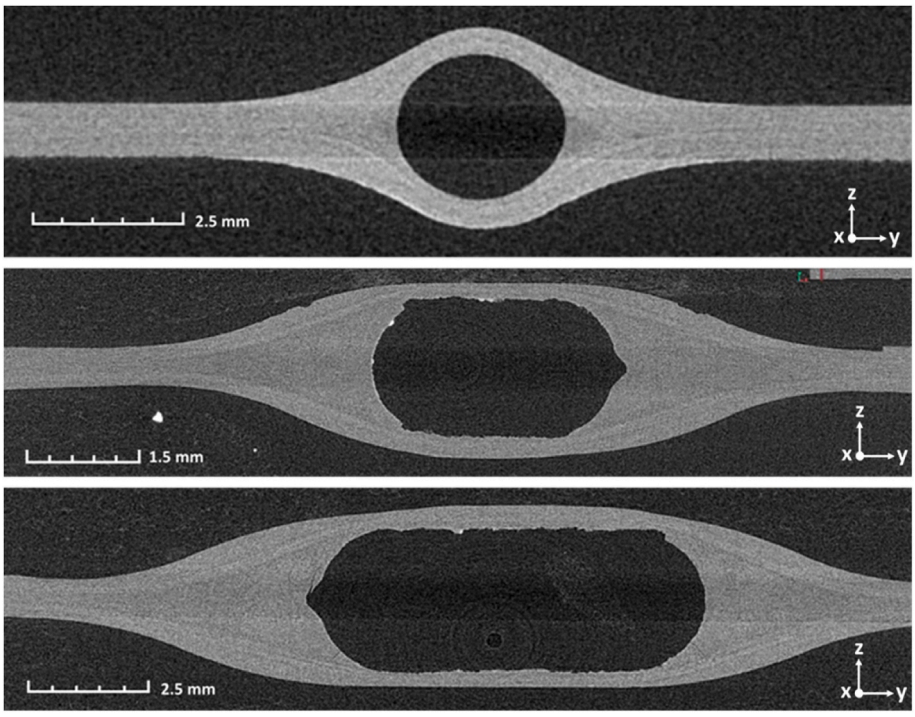

Fig. 10. Cross-section views obtained in the micro-tomography analysis of plates with embedded circular and oblong channels.

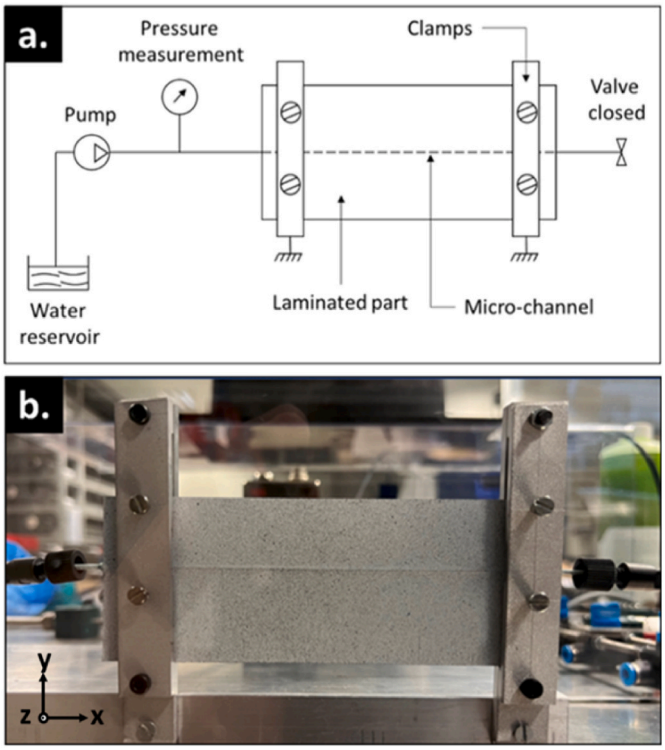

Fig. 11. (a) Hydraulic schematics of the experimental setup. (b) Test specimen with a random pattern for DIC installed in the test setup.

5. Tests results: pressure resistance of the laminates with embedded channels

5.1. Microstructure considerations

The microstructure at the vicinity of the channel is expected to play a key role in the failure process of the laminates.

Near the channel, the microstructure of the laminates depends on the first ply at either side of the mid-plane. With 90° plies (referred as 90°/90° interface), resin pockets around the channels are clearly visible (refer to Fig. 6a.). In contrast, with 0° plies (referred as 0°/0° interface) laminates show fibres migrating from the surrounding 0° plies towards the mid-plane (refer to Fig. 6b.). As for the T300 woven laminates, there is no evidence of fibre migration, resulting in the presence of resin pockets (refer to Fig. 6c.). The high bending stiffness about the longitudinal axis of the preform prevents both the 90° and woven plies from perfectly conforming to the shape of the PLA, resulting in the creation of a volume around the channel which is primarily filled by resin. In laminates with a 0°/0° interface, longitudinal fibres from the plies in contact with the preform are relatively free to move parallel to the PLA, so they are dragged towards the symmetry plane as the resin fills the volume surrounding the channel.

5.2. Pressure tests on laminates with unreinforced channels

Fig. 12a depicts the burst pressures obtained for laminates with 0°/0° and 90°/90° interfaces. A minimum of three samples were tested for each channel geometry (see **Section 2.2**). Due to the scatter observed in the results obtained for both $[90/0/90]_s$ and $[90/0/0/90]_s$ laminates with 1.75 mm circular channels, additional samples were tested to increase the statistics (twelve and ten samples respectively). Additional samples were required when the failure occurred in the connectors instead of the laminate. Fig. 12 only shows the results of burst pressures where the failure occurred in the laminates.

In addition, Fig. 13 shows the out-of-plane displacement (i.e. perpendicular to the lamination plane as defined by the z-axis shown in Fig. 5c.) results measured with the DIC system for laminates with 1.75 mm circular channels and both interfaces (i.e. 0°/0° and 90°/90°). For each case, the values depicted in the graphs represent the average of the DIC data collected along the centre line of the channels, considering a 35 mm region on either side of the midpoint of the sample (refer to Fig. 13b and d.).

0°/0° interface laminates. The results obtained for the samples with a

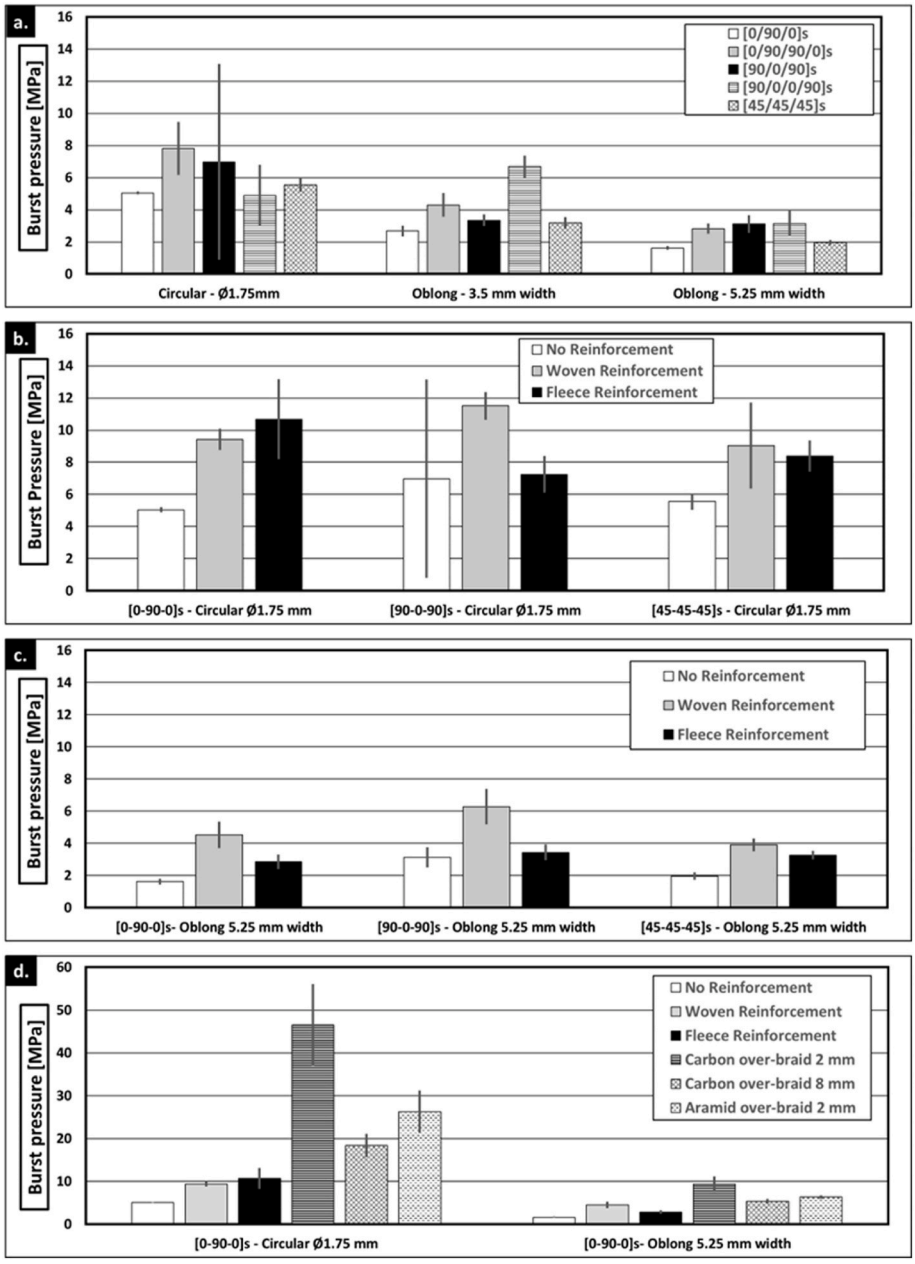

Fig. 12. (a) Average burst pressure results for unreinforced laminates with circular and oblong channels. (b) Average burst pressure results for reinforced laminates with carbon fleece and woven plies and 1.75 mm diameter circular channels. (c) Average burst pressure results for reinforced laminates with carbon fleece and woven plies and 5.25 mm wide oblong channels. (d) Average burst pressure results for reinforced and non-reinforced $[0/90/0]_s$ laminates with 1.75 mm circular and 5.25 mm oblong.

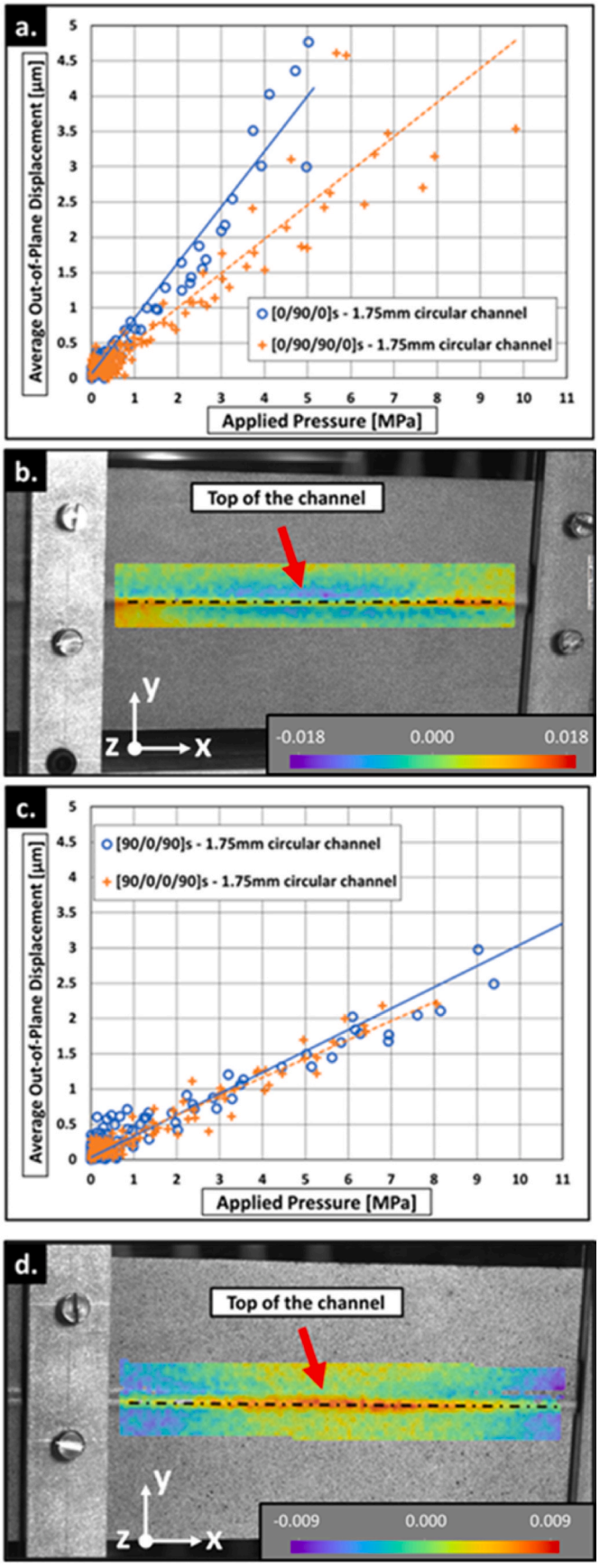

(caption on next column)

Fig. 13. (a) Average out-of-plane displacement along the centre line of the channel as a function of the applied pressure extracted from DIC data for $[0/90/0]_s$ and $[0/90/90/0]_s$ laminates with 1.75 mm diameter circular channels. (b) Typical DIC out-of-plane displacement field obtained for a $[0/90/0]_s$ laminate with 1.75 mm diameter circular channel. (c) Average out-of-plane displacement along the centre line of the channel as a function of the applied pressure extracted from DIC data for $[90/0/90]_s$ and $[90/0/0/90]_s$ laminates with 1.75 mm diameter circular channels. (d) Example of DIC out-of-plane displacement field obtained for a $[90/0/90]_s$ laminate with 1.75 mm diameter circular channel. Only a 35 mm region on either side of the midpoint of the samples has been considered to compute the average out-of-plane displacements.

0°/0° interface exhibited low scatter, indicating good repeatability in the manufacturing process. As expected, the burst pressure values were higher for the 8-ply laminates compared to their 6-ply counterparts. The increase in burst pressure ranged from 55 % for circular channels to 75 % for 5.25 mm wide oblong channels, as depicted in Fig. 14. Additionally, the experimental findings revealed that the width of the channels plays a significant role in the pressure resistance of the laminate, with narrower channels yielding greater resistance.

The DIC results depicted in Fig. 13a and b show higher deformations in the 6-ply laminates compared to the 8-ply laminates for the same applied pressure. This observation is consistent with the lower stiffness of the former. However, the out-of-plane displacement at the point of failure, estimated using the average burst pressures indicated in Fig. 12a. (5.04 MPa for 6-ply and 7.82 MPa for 8-ply laminates), was approximately the same in both cases, measuring around 4 µm.

90°/90° interface laminates. The burst pressure results for laminates with a 90°/90° interface exhibited a larger scatter than those obtained for samples with a 0°/0° interface regardless of the stack-up. This difference was particularly important for specimens with 1.75 mm diameter, circular channels. In Fig. 12a., it is evident that the pressure resistance of 6-ply laminates decreases as the channels widen. This trend is also observed for oblong channels embedded in $[90/0/0/90]_s$ plates, where performance surpasses that of their 6-ply counterparts. Surprisingly, the results for 8-ply specimens with 1.75 mm circular channels were inferior to both 3.75 mm wide oblong channels and 1.75 mm circular channels embedded in $[90/0/0/90]_s$ and $[90/0/90]_s$ laminates, respectively. Further investigations are required to understand the reasons for this unexpected trend, which are not yet fully understood.

As depicted in Fig. 13c and d., the average out-of-plane displacements for 6-ply and 8-ply laminates with a 90°/90° interface and a 1.75 mm circular channel are relatively similar, although the thinner samples exhibited slightly larger deformations. The out-of-plane displacement at the point of failure, estimated using the average burst pressures indicated in Fig. 12a. (6.97 MPa for $[90/0/90]_s$ and 4.89 MPa for $[90/0/0/90]_s$) is approximately 2 µm and 1.5 µm for the 6-ply and 8-ply laminates respectively. However, since these values are within the resolution of the DIC system, it is difficult to draw conclusions from these results. Further investigations and complementary analysis will be necessary in future studies.

T300 Plain weave laminates. The results of the T300 woven samples displayed a relatively low scatter, falling between the burst pressures obtained for the UD laminates with 0°/0° and 90°/90° interfaces. It is worth mentioning that resin pockets around the channels were observed in both the woven laminates and samples with a 90°/90° interface (refer to Fig. 6a and c.). This indicates that the scatter observed in the burst pressure results of the latter cannot be solely attributed to these resin pockets. Instead, it is plausible that the 90° plies may be more prone to damage during the lamination process, particularly in the transition section between the channel and flat regions of the composite plates.

5.3. Pressure resistance of laminates with reinforced channels

Additional plies of carbon fleece or T300 woven prepreg as well as

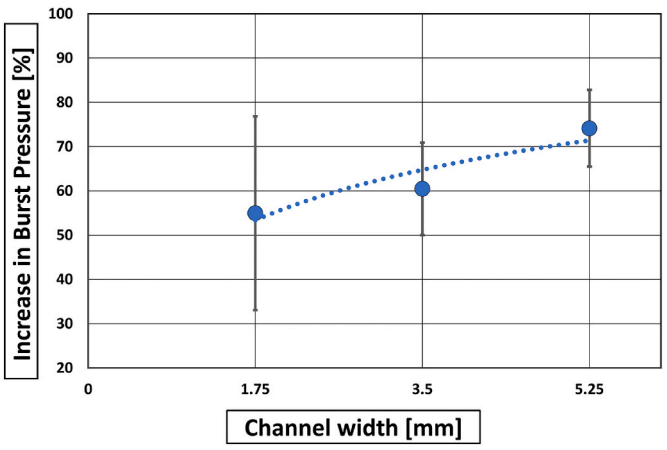

Fig. 14. Increase in burst pressure obtained with non-reinforced $[0/90/90/0]_s$ laminates compared to the $[0/90/0]_s$ laminates.

carbon and aramid over-braids were studied as potential reinforcements for the plates with circular and 5.25 mm wide oblong channels. Fig. 15 show the typical micro-structure of the manually reinforced plates. The fleece and woven plies exhibited discontinuities in the overlap area, while the braids (see Fig. 16) conformed well to the shape of the PLA preforms, resulting in high-quality channels. Braids with shorter laylengths led to smoother channel cross-sections and a more uniform fibre distribution around the channel (refer to Fig. 16a–c., and Fig. 17a–c.).

Laminates with carbon fleece and woven ply reinforcements. The burst pressure obtained with laminates reinforced with carbon fleece and woven plies are shown in Fig. 12b and c. In most cases, both materials enhanced the pressure resistance of the laminates. The carbon fleece had a limited impact on laminates with a circular channel and 90°/90° interface, but yielded gains ranging from 50 % to 120 % for all other configurations. The relatively modest enhancement can be partly attributed to the low fibre areal weight of carbon fleece used in this study. The woven plies, on the other hand, resulted in even greater improvements. For the circular channels, the pressure resistance increased by 60–90 %, and for the 5.25 mm wide oblong channels, it increased by 100–180 %. However, the lamination process for these samples posed some challenges, especially for the woven reinforcements. Manual wrapping of the plies around the circular PLA preforms led to defects around the channel, resulting in some scatter in the burst pressure results (see Fig. 15a.). Nevertheless, these tests demonstrated the feasibility of locally reinforcing the channel to enhance the pressure resistance of the laminates.

Laminates with carbon and aramid over-braid reinforcements. For a meaningful comparison, the over-braids were only tested on samples with circular and 5.25 mm wide oblong channels and a $[0/90/0]_s$ stack-up, as this configuration exhibited the lowest scatter in the unreinforced form. While woven and fleece reinforcements proved effective, the gains

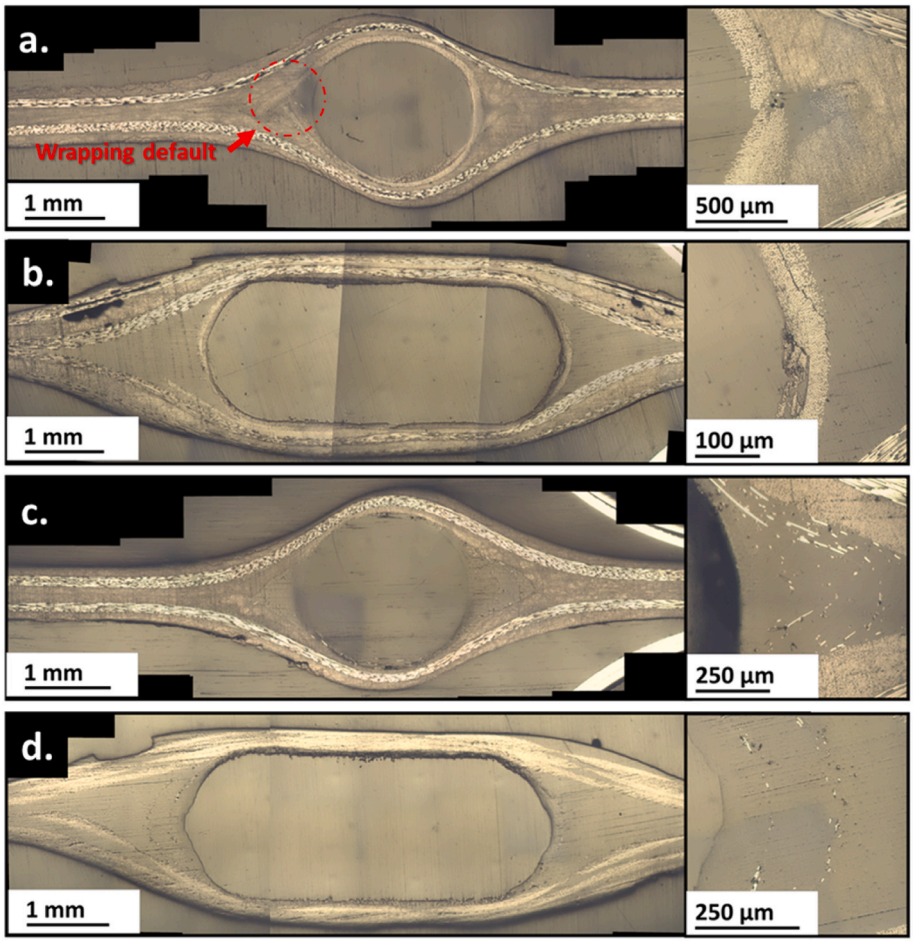

Fig. 15. Example micrographs of the laminates obtained with the carbon fleece and woven ply reinforcements manually wrapped around the PLA preforms. (a) Woven reinforcement in a 0°/0° interface laminate with a 1.75 mm diameter circular channel. (b) Woven reinforcement in a 90°/90° interface laminate with a 5.25 mm wide oblong channel. (c) Fleece reinforcement in a 0°/0° interface laminates with a 1.75 mm diameter circular channel. (d) Fleece reinforcement in a 90°/90° interface laminate with a 5.25 mm wide oblong channel.

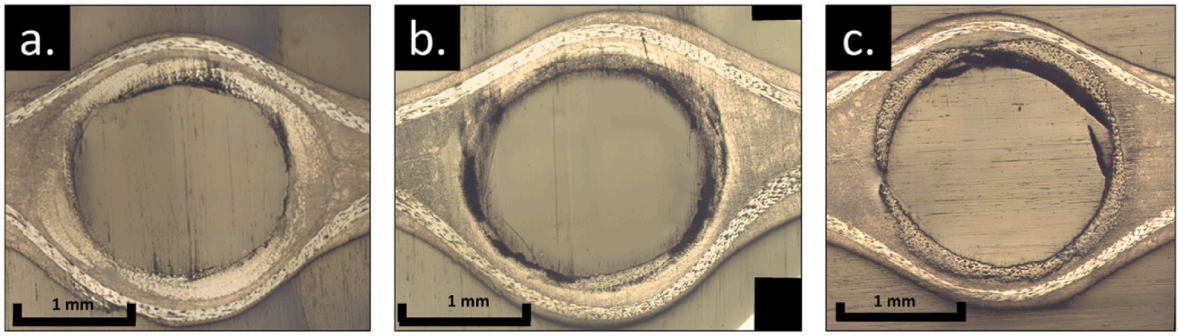

Fig. 16. Micro-structure of $[0/90/0]_s$ laminates with 1.75 mm diameter circular channels reinforced with (a) a carbon fibre over-braid with 2 mm lay-length, (b) a carbon over-fibre braid with 8 mm lay-length and (c) an aramid fibre over-braid with 2 mm lay-length.

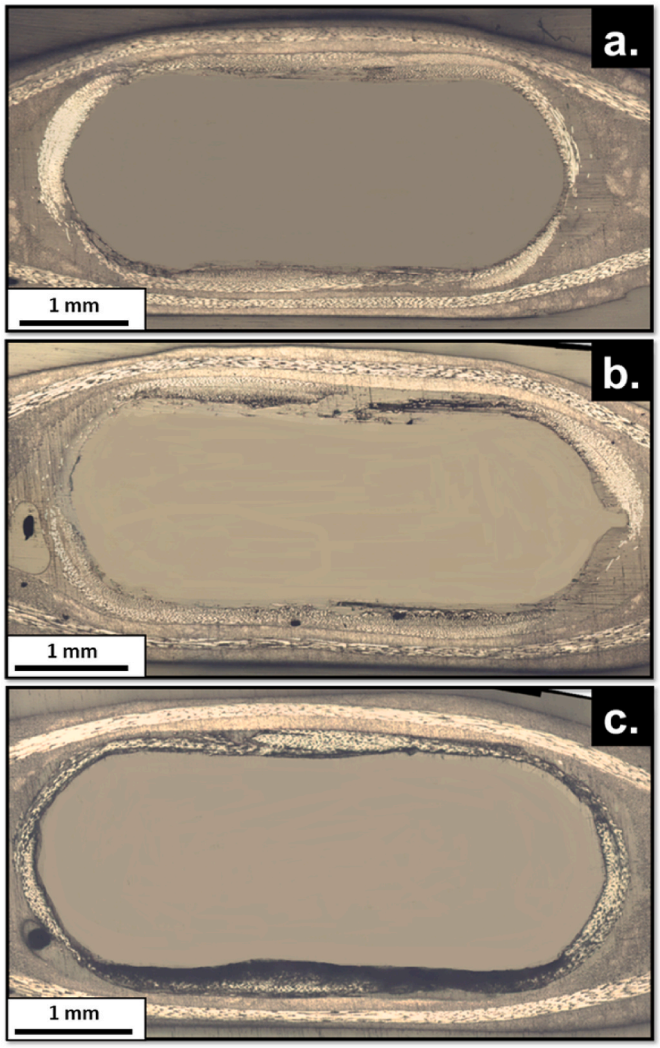

Fig. 17. Micro-structure of $[0/90/0]_s$ laminates with 5.25 mm wide oblong channels reinforced with (a) a carbon fibre over-braid with 2 mm lay-length, (b) a carbon over-fibre braid with 8 mm lay-length and (c) an aramid fibre over-braid with 2 mm lay-length.

achieved with the braids were more substantial (see Fig. 12d.). Carbon braids with a 2 mm lay-length resulted in an approximate 1000 % increase in the burst pressure of the laminates with circular channels. In comparison to the unreinforced configuration, carbon braids with an 8 mm lay-length and aramid braids with a 2 mm lay-length enhanced the pressure resistance by 360 % and 520 % respectively for circular channels. These results indicate that shorter lay-lengths are beneficial for the pressure resistance, and carbon fibre over-braids offer a clear performance advantage over aramid counterparts. Similar trends were observed for the 5.25 mm wide oblong channels with the over-braids. In this case, carbon braids with a 2 mm lay-length exhibited a 500 % increase in burst pressure compared to the unreinforced configuration, while the improvements obtained with the 8 mm carbon and 2 mm aramid braids were similar to those reported for the plates manually reinforced with an additional woven ply (see Fig. 12d.).

5.4. Analysis of failure process

After the pressure tests, the samples were examined using X-ray micro-computed tomography to assess the failure mode, paying special attention to identify the crack initiation point and the propagation path.

Laminates with unreinforced channels. Fig. 18 presents the typical failure patterns obserikved in laminates with both a 0°/0° interface (Fig. 18a and b.) and a 90°/90° interface (Fig. 18c and d.). In all these cases, the crack initiates in the resin-rich region surrounding the channel. Subsequently, in the laminates with a 0°/0° interface, it grows between the 0° and 90° plies. Conversely, in laminates with a 90°/90° interface, the crack propagates along the mid-plane of the sample. As a result, a large delamination area is formed (see Fig. 18e.).

Laminates with carbon fleece and woven ply reinforcements. The failure patterns observed in laminates with carbon fleece and woven plies (see Fig. 19a and Fig. 19b.) closely resemble those of the unreinforced samples. Crack initiation still occurs in the resin rich areas surrounding the channels, albeit at higher internal pressures. The additional plies do not significantly affect the overall crack propagation path, partly due to the limitations associated with manual wrapping around the PLA preform, which leads to local imperfections in the reinforcements in this region (see Fig. 15a.).

Laminates with carbon and aramid over-braid reinforcements. The laminates incorporating carbon and aramid braids exhibited a distinct failure pattern. In this case, crack initiation typically took place closer to the vertical symmetry plane (see Figs. 19c and 20a–f.) rather than in the resin-rich areas surrounding the channel. This shift in the initiation point demonstrates the effectiveness of the braids, explaining their ability to enhance the pressure resistance of the samples.

6. Conclusions

This study focused on the pressure resistance of composite laminates with embedded channels manufactured using sacrificial PLA preforms. Destructive tests were conducted to determine the burst pressure of the laminates as a function of the stacking sequence and the cross-section geometry of the channels. Circular and oblong channels were evaluated and various reinforcement techniques were investigated to enhance the pressure resistance of the laminates.

The highest average burst pressure obtained for unreinforced plates

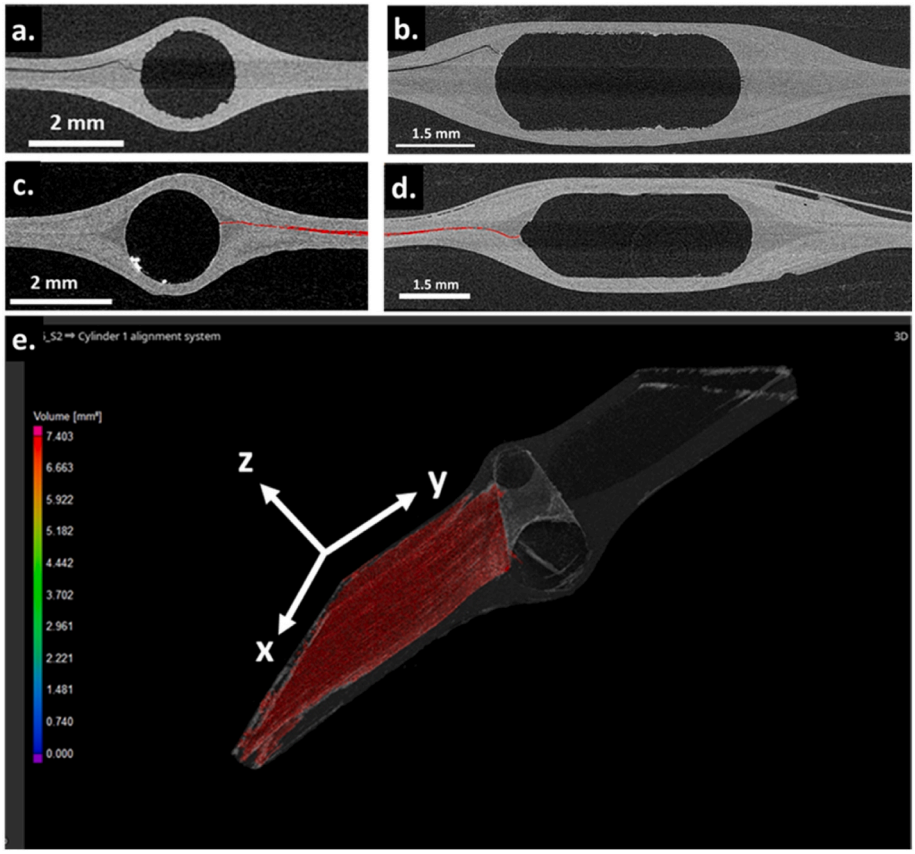

Fig. 18. Results obtained in the micro-tomography analysis of non-reinforced samples after the pressures tests. (a) Crack path in a laminate with a 0°/0° interface and 1.75 mm diameter circular channel. (b) Crack path in a laminate with a 0°/0° interface and 5.25 mm wide oblong channel. (c) Crack path in a laminate with a 90°/90° interface and 1.75 mm diameter circular channel. (d) Crack path in a laminate with a 90°/90° interface and a 5.25 mm wide oblong channel. (e) Example of the delamination surface (in red) in a test sample after failure.

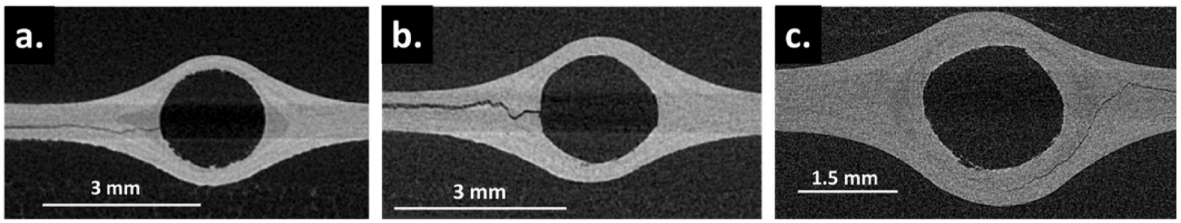

Fig. 19. Results obtained in the micro-tomography analysis of reinforced samples with 0°/0° interface and 1.75 mm diameter circular channels after the pressures tests. (a) Crack path in a laminate featuring a carbon fleece reinforcement. (b) Crack path in a laminate reinforced with a T300 woven ply. (c) Crack path in a laminate reinforced using a carbon fibre over-braid with 2 mm lay-length.

was 7.8 MPa, which occurred in $[0/90/90/0]_s$ laminates with 1.75 mm diameter circular channels. For 6-ply unreinforced stack-ups, the best average results (7.0 MPa) were achieved with circular channels and a $[90/0/90]_s$ layup. In general, narrower channels and thicker laminates tended to improve the pressure resistance. Laminates with a 90°/90° interface showed more variability in the results compared to those with a 0°/0° interface, regardless of the stack-up. This behaviour may be attributed to damage in the 90° plies during the lamination process, although further investigations are required to confirm this hypothesis.

The three types of reinforcement investigated in this study enhanced the pressure resistance of the laminates with embedded channels. Adding a carbon fleece or T300 plain weave ply manually wrapped around the PLA preform resulted in moderate increases in burst pressure, ranging from 50 % to 180 % compared to the unreinforced laminates. However, the most significant improvements were achieved with 2 mm lay-length carbon braids, which increased the pressure resistance by nearly 1000 % in 1.75 mm circular channels embedded in $[0/90/0]_S$ laminates (up to 45.7 MPa). Shorter lay-lengths proved to be beneficial for pressure resistance, and carbon fibre over-braids demonstrated superior performance compared to aramid counterparts.

Micro-graphic examinations and X-ray micro-computed tomography of the laminates revealed resin-rich areas around the channels. Crack initiation occurred in these regions when non-reinforced laminates were subjected to increasing internal pressure. The same applies to samples incorporating carbon fleece and woven plies as reinforcements. In contrast, the presence of the braids shifted the point of failure towards the vertical symmetry plane of the channels, explaining their ability to enhance the pressure resistance.

The findings of this study lay the groundwork for a better understanding of the behaviour of carbon composite plates with embedded channels under internal pressure. When implemented in numerical models, these findings could enable the prediction of failure in complex

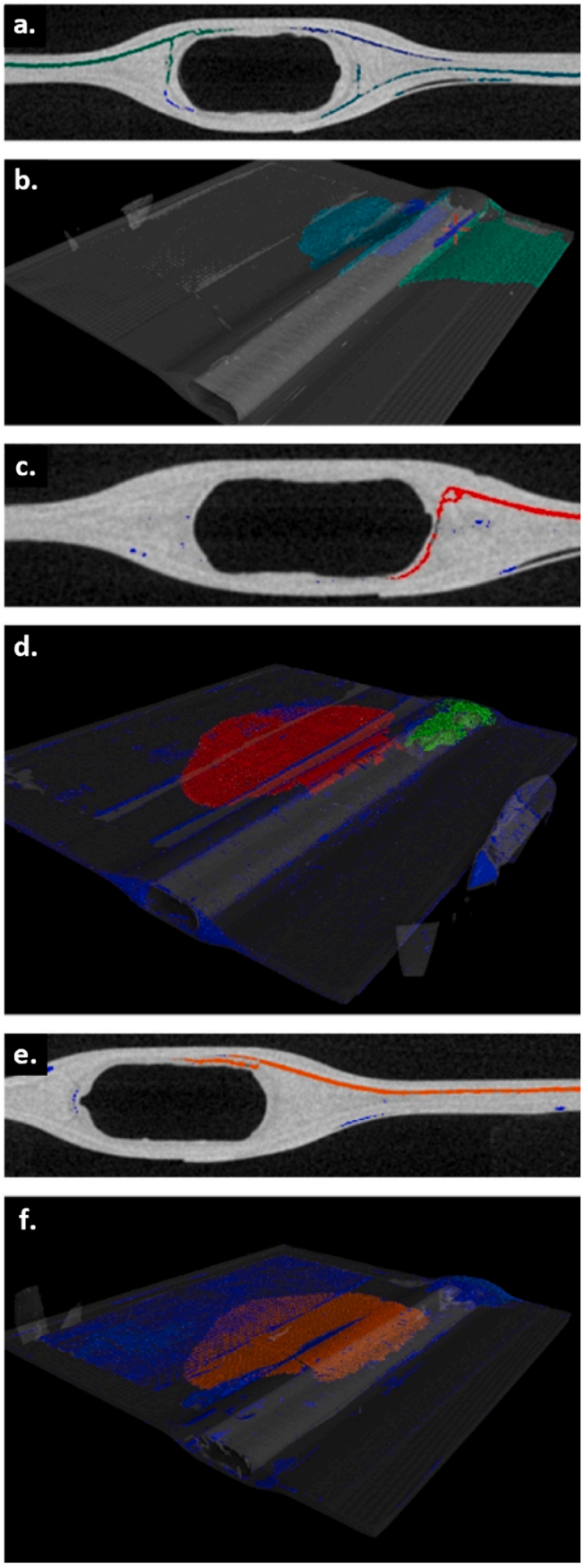

Fig. 20. Results obtained in the micro-tomography analysis of reinforced samples with 0°/0° interface and 5.25 mm wide oblong channels after the pressures tests. (a) Crack path in a laminate reinforced using a carbon fibre over-braid with 2 mm lay-length and (b) corresponding delamination surface (in green and blue) after failure. (c) Crack path in a laminate reinforced using a carbon fibre over-braid with 8 mm lay-length and (d) corresponding delamination surface (in red) after failure. (e) Crack path in a laminate reinforced using an aramid fibre over-braid with 2 mm lay-length and (f) corresponding delamination surface (in red) after failure.

vascular networks, opening the door for the use of this technology in future High Energy Physics applications.

6.1. Possible applications beyond active cooling in local supports

The use of channels directly embedded in laminate structures offers numerous potential applications.

In the case of active cooling, the combination of sacrificial PLA preforms and over-braiding reinforcements presents a promising approach to significantly enhance burst pressure, thereby meeting the requirements for HEP applications. Initial 40-h decay tests with laminates featuring circular channels and carbon over-braids have shown promising results under typical operation and design pressures for CO2 cooling systems (ranging from 20 bar to 160 bar). However, a thorough investigation into the long-term pressure-bearing capacity of vascularized composite plates is crucial. Additionally, further research is required to assess the effects of low temperatures and cyclic loads on their sustained performance. The permeability of the laminates, compatibility of the resin system with the cooling fluid as well as potential radiation effects must be well understood before such technology can be used in detector areas where reliability is paramount. The materials used in this study were not specifically chosen for these purposes and should be optimized accordingly. Over-braiding optimisations could be investigated to increase the pressure resistance and heat transfer. For larger channels, optimising the number or the size of tows could also lead to a better coverage of the fibre, improving the burst pressure. Moreover, the design of structures with embedded channels necessitates a robust numerical model to accurately predict failure. Work is underway in these areas.

Other potential HEP applications could be compatible with this technology. For example, dry-air distribution systems (i.e. controlled atmosphere) or active thermal barriers within the experiments. The fluids required for these applications are less demanding in terms of pressure than those used for low temperature on-detector cooling, making the implementation of this technology somewhat less challenging in the former. However, in these cases the optimal design of vascularized composite structures will require complex multi-channel networks, so further studies are necessary to examine potential interactions between adjacent channels and their impact on the overall mechanical resistance.

Out of the HEP sphere, this technology could find interest in various areas. For example, space and automotive industries already consider vascular channels for applications such as cooling solar panels or electric car batteries. Self-healing composite area could also find potential interest for healing agent distribution. This study complements the existing knowledge and provides the foundation for enhancing their ability to withstand high internal pressure.

CRediT authorship contribution statement

M. Dias: Writing – original draft, Validation, Methodology, Investigation, Formal analysis, Data curation, Conceptualization. **D. Alvarez:** Writing – review & editing, Validation, Supervision, Funding acquisition, Conceptualization. **F. Boyer:** Writing – review & editing, Validation, Supervision, Resources. **H. Lu:** Investigation. **P. Olivier:** Writing – review & editing, Supervision, Formal analysis. **L.R. Pickard:**

Investigation, Formal analysis. **B. Teissandier:** Supervision, Resources.

Declaration of competing interest

The authors declare that they have no known competing financial interests or personal relationships that could have appeared to influence the work reported in this paper.

Data availability

No data was used for the research described in the article.

Acknowledgements

This research work has been supported financially by the CERN Strategic Programme on Technologies for Future Experiments (WP4 - Mechanics). Dr Pickard kindly acknowledges funding for research including overbraiding provided by UK Engineering and Physical Sciences Research Council (EPSRC) programme Grant EP/T011653/1, Next Generation Fibre-Reinforced Composites: a Full Scale Redesign for Compression in collaboration with University of Bristol, and for this collaborative work by the University of Bristol International Strategic Fund.

References

[1] Home | CERN." https://home.web.cern.ch/(accessed April 17, 2023).
[2] Rossi L, Fischer P, Rohe T, Wermes N. Pixel detectors: from fundamentals to applications. In: Particle acceleration and detection. Berlin, Heidelberg: Springer; 2006. https://doi.org/10.1007/3-540-28333-1.
[3] Technical design report for the ATLAS inner tracker pixel detector. Geneva: CERN; 2017. https://doi.org/10.17181/CERN.FOZZ.ZP3Q.
[4] Abelev B, et al. Technical design report for the upgrade of the ALICE inner tracking system. 2014. https://doi.org/10.1088/0954-3899/41/8/087002.
[5] Tavlet M, Fontaine A, Schönbacher H. "Compilation of radiation damage test data. In: Index des résultats d'essais de radiorésistance. second ed.,". Geneva: CERN; 1998. https://doi.org/10.5170/CERN-1998-001.
[6] Backhaus M. The upgraded pixel detector of the ATLAS experiment for run 2 at the large Hadron collider. Nucl Instrum Methods Phys Res Sect A Accel Spectrom Detect Assoc Equip Sep. 2016;831:65–70. https://doi.org/10.1016/j.nima.2016.05.018.
[7] Dinardo ME. The pixel detector for the CMS phase-II upgrade. J Inst Met Apr. 2015; 10(4):C04019. https://doi.org/10.1088/1748-0221/10/04/C04019.
[8] Abbott B, et al. Production and integration of the ATLAS insertable B-layer. J Inst Met May 2018;13(5):T05008. https://doi.org/10.1088/1748-0221/13/05/T05008.
[9] Romagnoli G, et al. Silicon micro-fluidic cooling for NA62 GTK pixel detectors. Microelectron Eng Sep. 2015;145:133–7. https://doi.org/10.1016/j.mee.2015.04.006.
[10] Robitaille S, Patz G, Johnson S. Advanced composite stable structures, appropriate materials for high precision detectors. 1994. https://doi.org/10.5170/CERN-1994-007.115.
[11] Bungau C, et al. Induced activation in accelerator components. Phys. Rev. ST Accel. Beams Aug. 2014;17(8):084701. https://doi.org/10.1103/PhysRevSTAB.17.084701.
[12] Burchell TD. Radiation effects in graphite and carbon-based materials. MRS Bull Apr. 1997;22(4):29–35. https://doi.org/10.1557/S0883769400033005.
[13] Hoffman EN, Skidmore TE. Radiation effects on epoxy/carbon-fiber composite. J Nucl Mater Jul. 2009;392(2):371–8. https://doi.org/10.1016/j.jnucmat.2009.03.027.
[14] Aglieri Rinella G, et al. Strategic R&D programme on technologies for future experiments - annual report. 2021. https://doi.org/10.17181/CERN-EP-RDET-2022-006.
[15] Abada A, et al. FCC-Hh: the Hadron collider. Eur Phys J Spec Top Jul. 2019;228(4): 755. https://doi.org/10.1140/epjst/e2019-900087-0. 1107.
[16] Hellenschmidt D, et al. New insights on boiling carbon dioxide flow in mini- and micro-channels for optimal silicon detector cooling. Nucl Instrum Methods Phys Res Sect A Accel Spectrom Detect Assoc Equip Apr. 2020;958:162535. https://doi.org/10.1016/j.nima.2019.162535.
[17] Pety SJ, Tan MHY, Najafi AR, Barnett PR, Geubelle PH, White SR. Carbon fiber composites with 2D microvascular networks for battery cooling. Int J Heat Mass Tran Dec. 2017;115:513–22. https://doi.org/10.1016/j.ijheatmasstransfer.2017.07.047.
[18] Smart B. ATLAS pixel detector design for the HL-LHC. J Inst Met Feb. 2017;12(2): C02011. https://doi.org/10.1088/1748-0221/12/02/C02011. C02011.
[19] McElroy MW, Lawrie A, Bond IP. Optimisation of an air film cooled CFRP panel with an embedded vascular network. Int J Heat Mass Tran Sep. 2015;88:284–96. https://doi.org/10.1016/j.ijheatmasstransfer.2015.04.071.
[20] Demiral M, Tanabi H, Sabuncuoglu B. Experimental and numerical investigation of transverse shear behavior of glass-fibre composites with embedded vascular channel. Compos Struct Nov. 2020;252:112697. https://doi.org/10.1016/j.compstruct.2020.112697.
[21] Esser-Kahn AP, et al. Three-dimensional microvascular fiber-reinforced composites. Adv Mater 2011;23(32):3654–8. https://doi.org/10.1002/adma.201100933.
[22] Dong H, et al. Chemical treatment of poly(lactic acid) fibers to enhance the rate of thermal depolymerization. ACS Appl Mater Interfaces Feb. 2012;4(2):503–9. https://doi.org/10.1021/am2010042.
[23] Fan Y, Nishida H, Mori T, Shirai Y, Endo T. Thermal degradation of poly(l-lactide): effect of alkali earth metal oxides for selective l,l-lactide formation. Polymer Feb. 2004;45(4):1197–205. https://doi.org/10.1016/j.polymer.2003.12.058.
[24] Dalton B, Dixon D, Mcllhagger A, Archer E. Sacrificial component fabrication for optimised production of micro-vascular polymer composite. IOP Conf Ser Mater Sci Eng Feb. 2015;74(1):012005. https://doi.org/10.1088/1757-899X/74/1/012005.
[25] Garg M, White SR, Sottos NR. Rapid degradation of poly(lactic acid) with organometallic catalysts. ACS Appl Mater Interfaces Dec. 2019;11(49):46226–32. https://doi.org/10.1021/acsami.9b17599.
[26] Patrick JF, et al. Robust sacrificial polymer templates for 3D interconnected microvasculature in fiber-reinforced composites. Compos Appl Sci Manuf Sep. 2017;100:361–70. https://doi.org/10.1016/j.compositesa.2017.05.022.
[27] Garg M, et al. Rapid synchronized fabrication of vascularized thermosets and composites. Nat Commun May 2021;12(1):1. https://doi.org/10.1038/s41467-021-23054-7.
[28] Centellas P, et al. Energy-efficient manufacturing of multifunctional vascularized composites. J Compos Mater Feb. 2023;57(4):581–92. https://doi.org/10.1177/00219983221142353.
[29] Chen Z, Zhang X. Manufacturing multifunctional vascularized composites by through-thickness frontal polymerization and depolymerization: a numerical study on the impact of sacrificial fiber configurations. Compos Sci Technol Mar. 2024; 247:110394. https://doi.org/10.1016/j.compscitech.2023.110394.
[30] Olugebefola SC, et al. Polymer microvascular network composites. J Compos Mater Oct. 2010;44(22):2587–603. https://doi.org/10.1177/0021998310371537.
[31] Coppola AM. Thermal regulation of vascularized fiber-reinforced polymer matrix composites. Oct. 2015 [Online]. Available: https://hdl.handle.net/2142/88967. [Accessed 18 April 2023].
[32] Kousourakis A, Bannister MK, Mouritz AP. Tensile and compressive properties of polymer laminates containing internal sensor cavities. Compos Appl Sci Manuf Sep. 2008;39(9):1394–403. https://doi.org/10.1016/j.compositesa.2008.05.003.
[33] Kousourakis A, Mouritz AP, Bannister MK. Interlaminar properties of polymer laminates containing internal sensor cavities. Compos Struct Sep. 2006;75(1–4): 610–8. https://doi.org/10.1016/j.compstruct.2006.04.086.
[34] Saeed M-U, Li B-B, Chen Z-F. Mechanical effects of microchannels on fiber-reinforced composite structure. Compos Struct Oct. 2016;154:129–41. https://doi.org/10.1016/j.compstruct.2016.07.057.
[35] Pickard LR, Allegri G, Wisnom MR. Overbraiding of pultruded rods for hierarchical composites. In: In Proceedings of ICCM23 (23rd international conference on composite materials), 30 July-4 August; 2023. Belfast (UK), www.iccm-central.org/Proceedings/ICCM23proceedings/papers/ICCM_23_Full_Paper_348.pdf.
[36] Potter KD, Schweickhardt F, Wisnom MR. Impact response of unidirectional carbon fibre rod elements with and without an impact protection layer. J Compos Mater Sep. 2000;34(17):1437–55. https://doi.org/10.1106/3QGB-7PJ0-P129-4XRR.
[37] Pickard LR, Allegri G, Wisnom MR. Manufacturing advances for pultruded rod based structural members and thick ply systems: European conference on composite materials 2022. In: Proceedings of the 20th European conference on composite materials. B; Dec. 2022. p. 170–7. https://doi.org/10.5075/epfl-298799_978-2-9701614-0-0.
[38] The CMS phase-1 pixel detector upgrade. Geneva: CERN; 2020. https://doi.org/10.1088/1748-0221/16/02/P02027.
[39] Technical design report for the ATLAS inner tracker strip detector. Geneva: CERN; 2017. ATLAS-TDR-025.
[40] CIT Composite Materials Italy." Accessed: Jan. 30, 2024. [Online]. Available: https://www.composite-materials.it/pagina.php?cod=125.
[41] O'Keeffe C, Pickard LR, Cao J, Allegri G, Partridge IK, Ivanov DS. Multi-material braids for multifunctional laminates: conductive through-thickness reinforcement. Functional Composite Materials Feb. 2021;2(1):5. https://doi.org/10.1186/s42252-021-00018-0.